Design Against Tooth Interior Fatigue Fracture

Magnus MackAldener and Marten Olsson

Introduction

In a modern truck, the gear teeth are among the most stressed parts. Failure of a tooth will damage the transmission severely. Throughout the years, gear design experience has been gained and collected into standards such as DIN (Ref. 1) or AGMA (Ref. 2). Traditionally two types of failures are considered in gear design: tooth root bending fatigue, and contact fatigue. The demands for lighter and more silent transmissions have given birth to new failure types. One novel failure type, Tooth Interior Fatigue Fracture (TIFF), has previously been described by MackAldener and Olsson (Refs. 3 & 4) and is further explored in this paper.

Observations of TIFF

TIFF is characterized by a failure, approximately mid-height on the tooth, which distinguishes it from tooth root bending fatigue. Contact fatigue and/or spalling craters are not a prerequisite at the flank of a TIFF. In Figures 1 and 2, photos and a schematic of a typical TIFF can be seen.

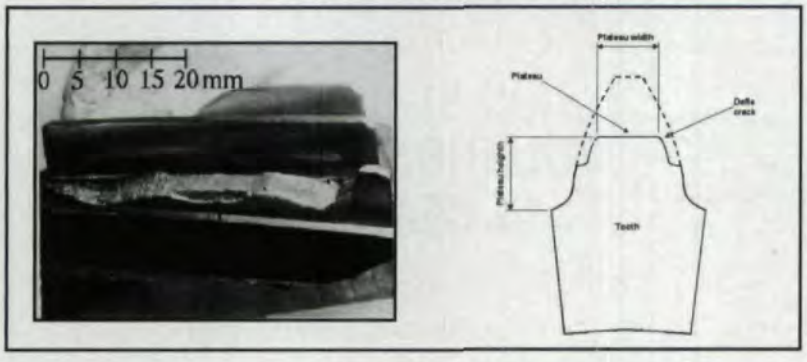

Fig. 1—A typical Tooth Interior Fatigue Fracture (TIFF) and a schematic of a TIFF.

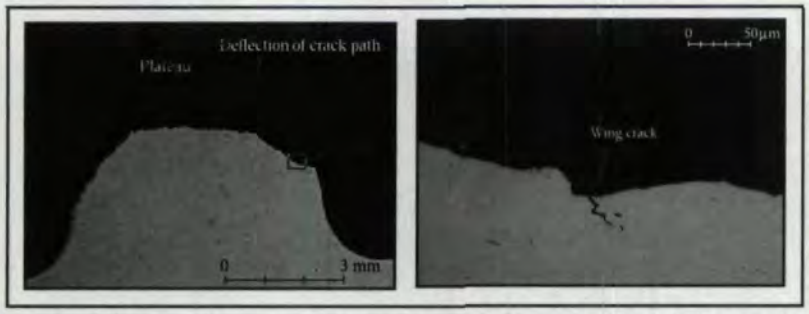

Fig. 2—Close-up of a cross-section of a TIFF. The wing crack indicates the propagation direction of the main crack (from the interior of the tooth towards the flank).

TIFF has been observed in case hardened idlers. A test series with idler wheels has been run. Out of 75 specimens, 20 were classified as TIFF. Tooth root bending fatigue or contact fatigue occurred in the other specimens.

TIFF Mechanism

TIFF is initiated in the interior of the tooth. Other known fatigue failures initiate at the surface. A failure type called Zahnkopfbruch in German, starting from spalling craters at the flank, has been reported by Shultz and Sauter (Ref. 5). Hence Zahnkopfbruch and TIFF are not the same type of failure, although they may appear similar. Alban (Ref. 6) described stress ruptures, which have a fracture surface similar to TIFF. However, stress rupture is not a fatigue fracture since the crack is formed during the hardening process.

TIFF is the result of: 1) constant residual tensile stresses in the interior of the tooth due to case hardening, and 2) alternating stresses due to the idler usage of the gear wheel.

Analysis

FE-model for mesh cycle simulation. To analyze the crack initiation process in the gear, a 2D FE-mesh was utilized. A plane strain 2D-mesh in the normal plane (perpendicular to the flank) was shown to give stress distributions in a cross-section of the tooth that is virtually the same as that of a 3D-mesh. Hence a 2D-mesh can be used for stress analysis of a complete mesh cycle. The FE-mesh is shown in Figure 3.

With a parametric model of the FE-mesh (developed in ANSYS, Ref. 7), an arbitrary position in the mesh cycle could be analyzed. The gear calculation program LDP (Ref. 8) computed the total force on one tooth as a function of position in the mesh cycle. The tooth force was divided by the width of the tooth and applied as torque.

The residual stress due to case hardening was found by applying an inelastic strain profile in accordance with residual stress measurements. The hardness penetration depth and its shape were obtained by hardness measurements.

Fatigue tests of the gear showed that shot peening increased the fatigue endurance limit by 36%.

Residual stress measurements of shot peened gear wheels showed that the shot peening increased the compression stresses to a depth of 0.1–0.2 mm.

Crack initiation criterion. In order to predict crack initiation in high cycle fatigue during multiaxial loading, Findley (Ref. 9) suggested a critical plane approach where the shear amplitude (τ_a) and the maximum normal stress ($\sigma_{n,max}$) during one load cycle are used to form the criterion. The criterion can be written

$$\sigma_F = \sigma_{crit} \quad (1)$$

where

$$\sigma_F = \tau_a + a_{cp}\sigma_{n,max} \quad (2)$$

is an equation for effective fatigue stress (Findley critical plane stress). The criterion states that crack initiation will occur if σ_F is greater than σ_{crit}. Here, σ_{crit} and a_{cp} are material constants that can be determined by combining the result of two fatigue tests. Here, σ_{crit} in the core was determined to be $\sigma_{crit,core}$ = 479.8 MPa while for the case, $\sigma_{crit,case}$ = 1090.0 MPa. The a_{cp} parameter was determined to be $a_{cp,core}$ = 0.37 and $a_{cp,case}$ = 1.00, respectively. Shot peening is considered in the FE-analysis by increasing the fatigue limit (σ_{crit}) 36% in the nodes of the model within 0.2 mm from the surface. The σ_{crit} and the a_{cp} parameter were taken to vary continuously between the case and core in the same manner as the hardness profile.

Numerical analysis. The FE-analysis is carried through in two stages: 1) calculation of the state of stress history in the tooth during one load cycle, including residual stresses, and 2) evaluation of the risk of crack initiation. The engaging gear teeth are analyzed in 19 different points of the mesh cycle, each point representing a "frozen" moment in the mesh cycle. The points included nine points with contact on each flank and one with the tooth unloaded. Results of the 19 analyses are combined to represent one load cycle (i.e. one revolution of the idler). The Findley critical plane stress is formed for every degree of plane inclination at each node of the cross-section of the loaded tooth. The maximum Findley critical plane stress at each node is stored for evaluation purposes.

Numerical results. In order to judge the risk of crack initiation, the crack initiation risk factor (CIRF) must be calculated. This is done by dividing the Findley critical plane stress by the σ_{crit} value at every material point. A contour plot of the CIRF of the gear can be seen in Figure 4b. It is also interesting to compare the CIRF for the studied gear used as an idler and in a single stage gear. The comparison can also be seen in Figure 4.

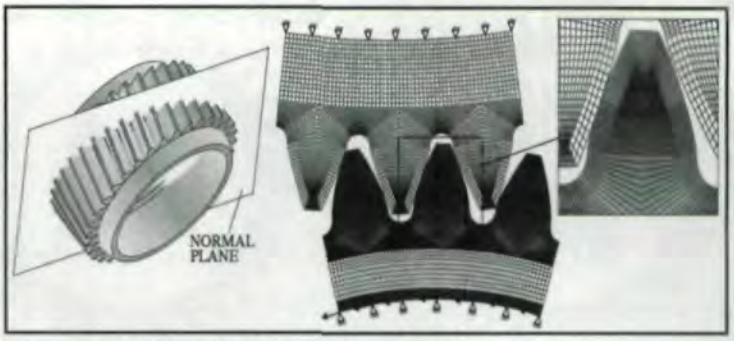

Fig. 3—Two-dimensional finite element mesh.

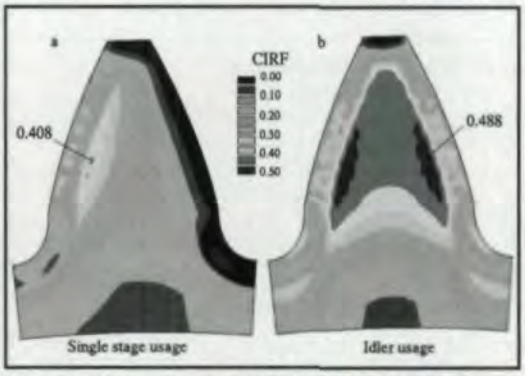

Fig. 4—Comparison of CIRF. a) the studied gear used as a single stage gear, b) the studied gear used as an idler.

The region with high CIRF is located approximately mid-height of the tooth and slightly below the case-core boundary. Thus, if a crack is developed in the interior of the tooth, it will initiate between the center-line and the case layer. The CIRF in the interior is increased by 20% if the gear is used as an idler instead of as a single stage gear. Moreover, the area (or volume) with high CIRF is larger in case of idler usage. Analysis of the risk of TIFF at different loads shows that, as the tooth load is increased, it is more likely to have a crack initiating in the root than in the interior. Thus, TIFF is a presumptive failure mode occurring at medium load, i.e. the load level is between the load at which contact fatigue is achieved and the load at with tooth root bending fatigue is obtained. This agrees well with the experience from the rig test of the idler gear.

Parameter Study

Crucial for a successful gear design is that the designer understands how different design parameters influence the response (certain properties) of the structure. Such knowledge can be gained by a factorial design. In contrast to a "one-factor-at-a-time" approach, the factorial design also gives information about interaction effects. For a detailed discussion on factorial design, see Box et al. (Ref. 10) or Montgomery (Ref. 11).

Here, a factorial design with five factors (A to E) was conducted. The parameters are the two material constants σ_{crit} (A) and a_{cp} (B), the slender-

Magnus MackAldener

(M. Sc., Lic. Eng.) received his degree in Vehicle Engineering at the Royal Institute of Technology (KTH) of Stockholm, Sweden, in 1995. Since 1997, he has been an industrial Ph.D. student at Scania, Europe's third-largest heavy truck manufacturer, and at the department of Machine Design at KTH. His research focus is on the exploration of fatigue phenomena in gears, as well as robust gear design. At Scania, he works at the department for Transmission Development, where he is doing structural analysis.

Marten Olsson

(M. Sc., Ph.D., Docent) is Associate Professor and Director of Undergraduate Studies at the Department of Solid Mechanics, Royal Institute of Technology, Stockholm, Sweden. His research background includes analysis of toughening mechanisms for ceramics, thermal cycling of ceramic reinforced metal matrix composites, wear resistance of FGMs and contact fatigue of case-hardened steels. Current research concerns fatigue initiation and propagation, both from a fundamental point of view and in applications. He cooperates with the Scania truck company regarding contact related fatigue in transmissions.

Fig. 5—The slender (left) and not-slender (right) geometry compared with the geometry of the original tooth (middle).

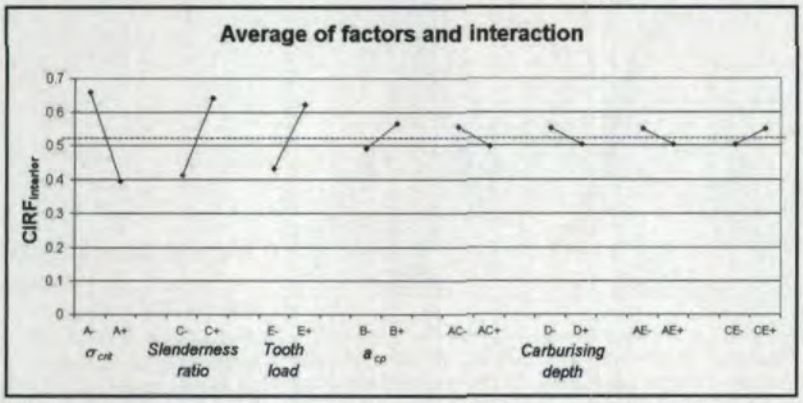

Fig. 6—The average of the factors with most influence on the CIRF in the interior. The overall mean is marked by the dashed line.

Table 1. The factors (parameters) and their levels.

Factor	Description	Low level (–)	High level (+)
A	σ_{crit} in core	359.85	559.75
B	a_{cp} parameter in core	0.28	0.46
C	Slenderness ratio	1.16	1.65
D	Carburizing depth	0.9 mm	1.5 mm
E	Tooth force	1238 Nm*	2064 Nm*

* Tooth force corresponding to torque on the idler in original design.

ness ratio, C (defined as the ratio between the height of the involute $((d_a-d_{Ff})/2)$ and the tooth thickness (s_{yn}) half-way between the transition from root fillet to involute (d_{Ff}) and the addendum diameter (d_a)), the carburizing depth (D) and the tooth load (E). For each factor, two levels were assigned, one low (marked with a minus sign) and one high (marked with a plus sign). The low and high level of each factor is set to approximately 75% and 125%, respectively, of the value of the original (previously analyzed) design of the studied gear. In Figure 5, the slender and not-slender gear design are compared with the geometry of the original gear wheel.

For details about the tooth geometry, see Table 3. The levels of the factors are given in Table 1.

Here, 32 experiments were conducted in accordance with an ordinary L32 orthogonal array. Each "experiment" in the array is represented by an FE-analysis determining the CIRF in the interior of the tooth.

Result of the parameter study. The result of the factorial design is the CIRF (response) in the interior of the tooth denoted y_i for the ith experiment (Table 4). Emanating from the results it is possible to estimate the main effect. The main effect should be interpreted as the change in response while changing the level of the factor from low to high. The main effect is given by

$$m_{N+} = \frac{1}{k^+}\sum_{i=1}^{k^+} y_{i+} - \frac{1}{k^-}\sum_{i=1}^{k^-} y_{i-} \qquad (3)$$

where k+ and k– are the number of times the factor appears at high and low level, respectively. The result of the factorial design is summarized in Table 2.

In Figure 6 the average of the factors regarded as significant is plotted. The main effect is the difference between the low (–) and high (+) level for each factor.

The greatest influence on the CIRF in the interior of the tooth comes from the factors A (σ_{crit}), C (slenderness ratio), E (tooth load) and B (a_{cp}) in that order. The influence on the CIRF in the interior from the factor D (the carburizing depth) is less than 5% but, somewhat unexpected, it is negative. This means that the lower the carburizing depth, the higher the risk of TIFF. It is also worth noting that the influence from the carburizing depth (factor D) is less than the interaction effect of σ_{crit} (factor A) and the slenderness ratio (factor C).

Since it is desirable to have as low a CIRF as possible, the optimal settings of the factors are A+, B–, C– and E–, meaning high σ_{crit} in the interior of the tooth, low slenderness, low tooth load and low a_{cp}.

Engineering Design Method

What so far has been shown in the present paper is that it is possible to predict and analyze TIFF by applying the FEM. However, this is time consuming and not appropriate in the design stage of gear development. Therefore, an "engineering

design method" (EDM) was developed and implemented in MatLab.

A design method based on superposition of elementary solutions. Two basic assumptions are assumed for the EDM. These are:

i) The critical Findley plane is assumed to be perpendicular to the center-line of the tooth.

ii) Stresses in the tooth interior are expressed using elementary solutions of elasticity theory. Normal stresses are estimated by beam theory. Shear stresses are estimated with the half-space solution combined with beam theory.

Basically, three types of superimposed stress states, acting on the pre-assumed critical plane, need to be considered. These are i) residual stresses due to case hardening ii) normal tension stresses due to bending and iii) shear stresses.

Residual stress. A beam (or rod) with varying cross-section can approximate the tooth in the residual stress estimation. In a surface layer with thickness dc_{eqv}, a constant volume expansion ε_h is prescribed. A sketch of the simplified tooth can be seen in Figure 7.

The width of the tooth is b, the height is h and the varying tooth thickness as a function of the diameter d_y is given by $s_{yn}(d_y)$. The stress in the y-direction in the interior of the tooth can be neglected. By assuming that stresses are homogenous in case and core, respectively, and combining equilibrium and Hooke's law in the x- and z-direction of the tooth, the following expression of residual stress is derived:

$$\sigma_{x,core} = \sigma_{res}(\hat{d}_y) = 2E\varepsilon_h dc_{eqv} \frac{(s_{yn}(\hat{d}_y) - 2dc_{eqv} + b)}{s_{yn}(\hat{d}_y)b(1-\nu)} \quad (4)$$

Equation 4 is valid at the center line of the tooth, but FE-calculation has shown that the residual stress in the x-direction of the tooth is fairly constant over a region on both sides of the center line. Therefore, Equation 4 can be taken to hold for the interior of the tooth not only at the center line.

Normal stress due to tooth load. Consider a gear tooth as in Figure 8. Here, d_{ev} is the bottom diameter of the active flank, d_a is the addendum and d_y is an arbitrary diameter. $F(d_y)$ is the total tooth force as a function of the diameter. The maximum normal stress at a point P at diameter $\hat{d}_y$ a distance $\hat{z}_b$ from the center line is given by:

$$\sigma^P{}_{normal} = \sigma^P{}_{bend} - \sigma^P{}_{compr} = \frac{M^{max}}{I(\hat{d}_y)}\hat{z}_b - \frac{F_N(d_y)}{b \cdot s_{yn}(d_y)} \quad (5)$$

where

$$M^{max} = \max\left\{F_T(d_y)(d_y - \hat{d}_y)\frac{1}{2}\right\} \; d_y > \hat{d}_y \quad (6)$$

Table 2. The main effects of the factors for the response $CIRF_{interior}$

Factor	Description	Main Effect
A	σ_{crit}	–0.264
B	a_{cp} parameter	0.072
C	Slenderness ratio	0.228
D	CD	–0.049
E	Tooth force	0.189

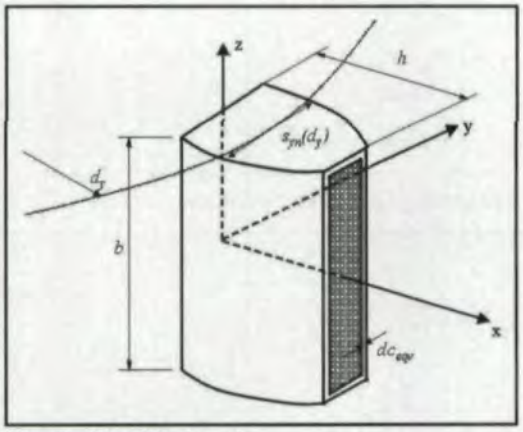

Fig. 7—Simplified tooth.

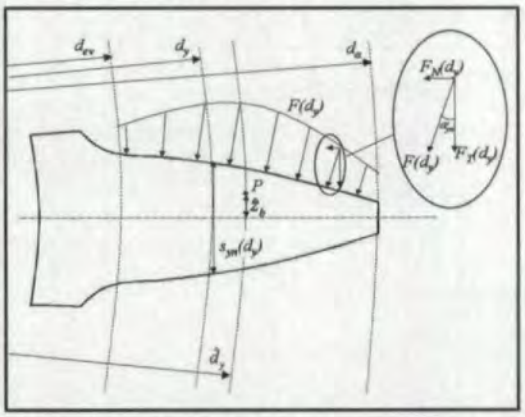

Fig. 8—Tooth load on gear tooth.

Shear stress. In estimating the shear stress amplitude at point P due to the tooth force, a pure beam analogy does not result in an acceptable estimate. The stress distribution, according to Johnson (Ref. 12), in an elastic half-space, as in Figure 9, due to a line load is given by

$$\tau_{xz}{}^{l} = -\frac{2F}{\pi b}\frac{xz^2}{(x^2+z^2)^2} \quad (7)$$

However, the half-space solution will result in stresses on the tooth boundaries (Ω_1 and Ω_2) that are not present in the real case (i.e. free surfaces are always stress free).

Since linear elasticity is assumed, superposition can be utilized and the error of the non-stress free boundaries can be compensated for. The method is to superimpose a stress state on the elastic half-space solution that eliminates the stresses at the boundaries (i.e. subtract boundary stresses). In order to simplify the computation,

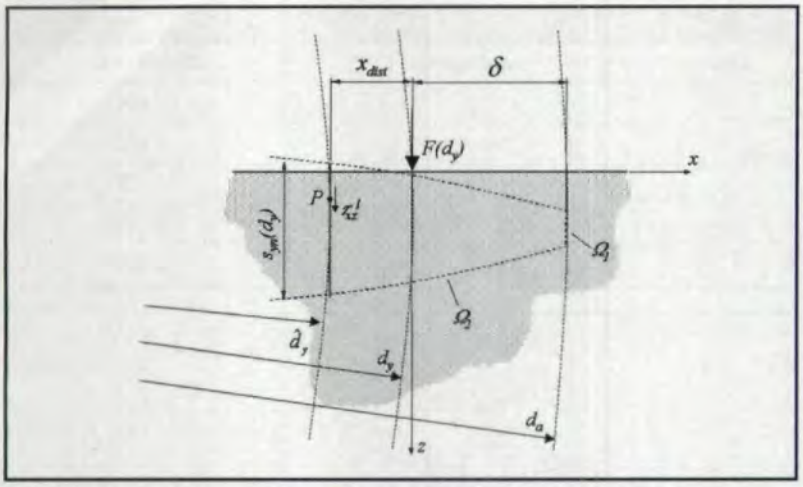

Fig. 9—Elastic half-space estimation of the contact problem in the tooth.

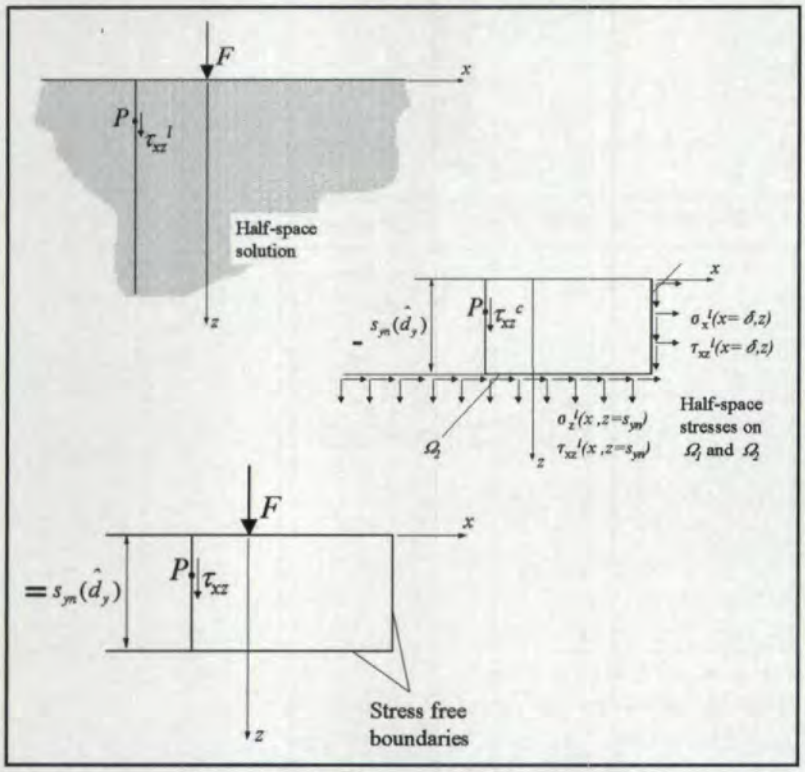

Fig. 10—Superposition of elastic half-space solution and compensating solution.

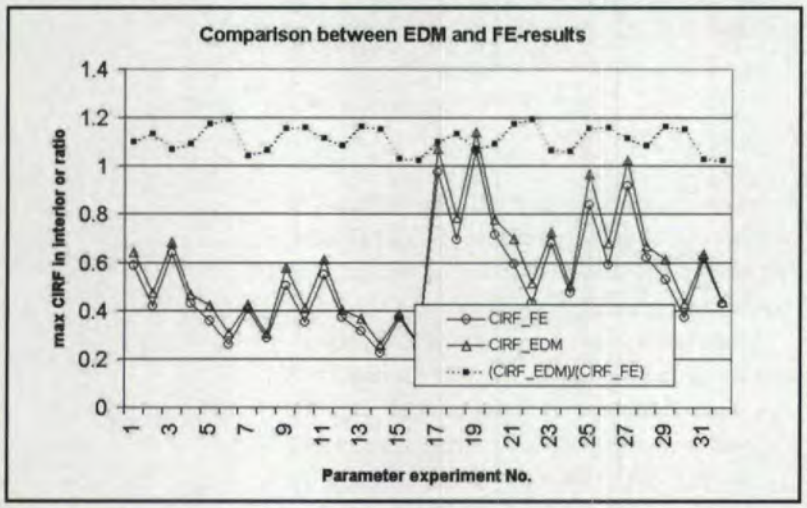

Fig. 11—Comparison of the CIRF calculated with the engineering design method and the CIRF according the FE-calculations in the parameter study.

the tapered tooth is approximated by a beam with constant thickness. The superposition technique is illustrated in Figure 10.

Consider the compensating solution (in Figure 10). The stresses on Ω_1 and Ω_2 in the compensating solution are given by the half-space solution (n Figure 10). After subtraction, stress free boundary conditions are fulfilled. The shear stress due to the line load on the half-space has been presented. The shear stress due to the compensation solution may be estimated by beam theory. The transverse force (T) on the studied plane in which point P lays is given by integrating the compensating solution along the boundaries Ω_1 and Ω_2. The latter integration should only be performed from the tooth tip to the studied plane in which P lays. The contributions to T from the two boundaries should be added to make up the transverse force. The transverse force at P is given by

$$T = T_1 + T_2 = \int_0^{s_{yn}} \tau_{xz}^{\ l}(x=\delta,z)bdz + \int_{-x_{dist}}^{\delta} \sigma_z^{\ l}(x,z=s_{yn})bdx = \ldots = \quad (8)$$

$$= \frac{F}{\pi}\left[\frac{x_{dist}\, s_{yn}(\hat{d}_y)}{(x_{dist}^{\ 2} + s_{yn}(\hat{d}_y)^2)} - \arctan\left(\frac{s_{yn}(\hat{d}_y)}{x_{dist}}\right)\right]$$

where $x_{dist} = (d_y - \hat{d}_y)/2$ and $\delta = (d_a - d_y)/2$. The shear stress due to the compensating solution, estimated as bending shear stress due to the transverse force T, is then given by

$$\tau_{xz}^{\ c} = \frac{TS(\hat{z}_b)}{I(\hat{d}_y)b} \quad (9)$$

where $S(\hat{z}b)$ is the static moment given by

$$S(z_b) = \int_{\hat{z}_b}^{s_n(\hat{d}_y)/2} z_b b dz_b = b\left(\frac{S_{yn}(\hat{d}_y)}{2} - \hat{z}_b\right)\left(\frac{S_{yn}(\hat{d}_y)}{2} + \hat{z}_b\right)\frac{1}{2} \quad (10)$$

However, it should be noted that the compensating shear stress should only be subtracted if the tooth force is positioned outside the studied plane (i.e. $d_y > \hat{d}_y$). The resulting shear stress at point P in a plane at $\hat{d}_y$ is thus given by

$$\tau_{xz}^{\ P} = \tau_{xz}^{\ l} - \theta(d_y - \hat{d})\,\tau_{xz}^{\ c} \quad (11)$$

where θ is the Heaviside's step function. However, in the Findley critical plane criterion, it is the shear stress amplitude rather than the shear stress itself that is used. Therefore, the maximum and minimum shear stress at each point is sought. It is not obvious when during the load cycle the maximum

and the minimum occurs, respectively. By implementing the derived expressions in a computer program (here MatLab is used), it is possible to determine the maximum and minimum shear stress at all points in the tooth interior, and the shear stress amplitude can be formed by

$$\tau_a^P = \frac{\max\{\tau_{xy}^P\}_{loadcycle} - \min\{\tau_{xy}^P\}_{loadcycle}}{2} \quad (12)$$

Findley stress. The total stress in the radial direction of the tooth (or in the x-direction as in Figure 7) is the sum of the residual stress and the bending stress. Consequently, the Findley critical plane stress can estimated by

$$\sigma_F^P = \tau_a^P + a_{cp,core}(\sigma_{res} + \sigma^P_{normal}) \quad (13)$$

The bar over the σ_F indicates that this is the EDM approximation of the Findley stress. By scanning through all plane diameters and all distances from the center line, the point in the interior of the tooth with maximum Findley stress can be determined.

Comparison with FEM results

The total tooth force as a function of contact force diameter is determined by the gear computation program LDP (Ref. 8). $F(d_y)$ is then approximated by a fourth-order, least-square fit to the calculated tooth force.

In order to verify the engineering design method, a comparison with an FE-analysis was conducted. Since an evaluation of the CIRF for different gear geometries is already made in the parameter study, it is possible to make a comparison for different geometries and parameter combinations. The previously conducted FE-analysis has shown that the area in the interior of the tooth with the highest Findley stresses is close to the case-core boundary (i.e. at depth CD). In the analysis, dc_{eqv} = 1.2 mm and ε_h = 0.000833 are used. In Figure 11, a comparison of the CIRF calculated with the engineering design method (CIRF_EDM) and the CIRF according the FE-computations (CIRF_FE) in the parameter study is shown.

It is clear from Figure 11 that the overall correlation between the CIRF calculated by the EDM and by FEM is good. It is noticed that the EDM overestimates the CIRF. The average discrepancy for all 32 investigated parameter configurations is 11% and never greater than 20%.

Discussion

The FE-analysis showed that the hypothesis of TIFF presented in this paper was strengthened. The parameter study surprisingly showed that the risk of TIFF was decreased as the carburizing depth was increased. This unexpected relation can be understood if the bending stress in the tooth is considered. The FE-analyses show that the region in the tooth with the highest CIRF is in the case-core boundary. Also, when the carburizing depth is low, the layer with the compressive stresses is thin and hence, the bending stress in the case-core boundary is greater due to the greater distance from the center line. The conclusion is that the effect of the bending stress is greater than the effect of the residual tensile stress in the interior of the tooth.

The parameter study also showed that the two factors having the greatest influence on the risk of TIFF are σ_{crit} in the interior of the tooth and the slenderness ratio. This highlights a new problem when it comes to gear design. When optimizing gears for noise, usually the slenderness ratio is increased, since slender gears allow higher contact ratio and potentially more silent gears. Therefore, TIFF has to be considered as a possible failure mode in future gear design.

Conclusions

In this work, the gear tooth failure mode TIFF is described and analyzed. In the analysis, FE-computations are utilized in conjunction with the Findley critical plane initiation criterion in order to predict crack initiation. It is shown that the TIFF cracks are initiated in the interior of the tooth. Other results are:

- The region where the interior crack will initiate is located approximately mid-height of the tooth and slightly below the case-core boundary.
- TIFF is a possibility at loads lower than the load where tooth root bending fatigue is achieved and at loads higher than the load where contact fatigue occurs.
- By using the gear wheel as an idler instead of as a single stage gear, the risk of TIFF is increased by 20%.

A parameter study was conducted in order to investigate which geometric and material parameters influenced the risk of TIFF. The parameter study was performed as a factorial design. The key results from the study are:

- The parameters influencing the risk of TIFF mostly are σ_{crit} in the interior, the slenderness ratio and the tooth load. The lower the σ_{crit}, the more slender the tooth and the higher the load, the greater the risk of TIFF.
- The influence from the a_{cp} parameter in the interior is small but positive, meaning the higher the a_{cp}, the greater the risk of TIFF.
- The influence of the carburizing depth on TIFF

Appendix—Gear data for gears in the factorial design.

The gear data of the two gear designs in the factorial design are given in the table below. For comparison, the gear data of the original design of the gear is given in Table 3. A sketch of the different gear designs is given in Figure 5. In Table 4, the crack initiation risk factors are presented as they were computed by FEM in the 32 experiments in the factorial design.

Table 3. Gear data of the slender (left) and not-slender (right) geometry compared with the geometry of the original tooth (middle).

	Slender gear design		Original gear design		Not-slender gear design	
	Pinion	Wheel	Pinion	Wheel	Pinion	Wheel
Modulus (mm)	2.34		3.06		3.75	
Pressure angle (°)	17.5		20		22.5	
Helix angle (°)	15		15		15	
Tooth width (mm)	43	35	43	35	43	35
Center distance (mm)	166.5		166.5		166.5	
Number of teeth	45	93	34	70	27	56
Addendum modification coefficient	0.270	–0.669	0.265	0.250	0.600	0.895
Diameter of addendum (mm)	116.5	230.6	116.5	230.6	116.5	230.6
Protuberance (mm)	0.060	0.095	0.060	0.060	0.60	0.060
Addendum for tool (mm)	4.850	3.900	4.350	4.350	4.350	4.800
Protuberance angle (°)	5.044	8.342	3.045	3.045	4.308	3.786
Radius of addendum for tool (mm)	0.45	0.85	1.20	1.20	1.75	1.45
Ratio	2.067		2.059		2.074	

Table 4. Crack initiation risk factors (CIRF) at the root and the interior of the tooth as they were computed by FEM in the factorial design.

Experiment	$CIRF_{root}$	$CIRF_{interior}$
1	0.757	0.586
2	0.449	0.417
3	0.752	0.640
4	0.437	0.429
5	0.206	0.358
6	0.105	0.259
7	0.203	0.408
8	0.100	0.285
9	0.757	0.503
10	0.449	0.353
11	0.748	0.550
12	0.437	0.372
13	0.206	0.317
14	0.105	0.224
15	0.203	0.371
16	0.100	0.257
17	0.720	0.976
18	0.380	0.695
19	0.780	1.066
20	0.390	0.715
21	0.206	0.596
22	0.105	0.432
23	0.203	0.681
24	0.100	0.476
25	0.690	0.839
26	0.430	0.589
27	0.750	0.917
28	0.430	0.620
29	0.206	0.529
30	0.105	0.373
31	0.203	0.619
32	0.100	0.428

is small, and the risk of TIFF is lower for a high carburizing depth than for a low carburizing depth.

An engineering design method (EDM) for design against TIFF was developed, implemented in MatLab and compared with the FE-calculations in the parameter study. The following results were found:

- It is possible to estimate the risk of TIFF by the EDM very quickly and with acceptable accuracy.
- The EDM overestimates the CIRF in the interior of the tooth compared to the FE-result by an average of 11%.

Acknowledgements

This work was supported by the Swedish Research Council for Engineering Science (TFR). Thanks are directed to Arne Larsson at Scania for invaluable help in the field of gear design and gear manufacturing. The authors thank Gunnar Strandell at Scania for encouragement and for the possibility to present this research, and they also thank Prof. Sören Andersson at KTH for support and guidance. ⚙

References

1. DIN (Deutsche Institut für Normung) 3990 Teil 3 (1987). *Tragfähigkeitsberechnung von Stirnrädern.*
2. AGMA Standard 2003-A86 (1982). *AGMA Standard* for *Rating the Pitting Resistance and Bending Strength of Spur and Helical Involute Gear Teeth.*
3. MackAldener M. and M. Olsson, "Interior Fatigue Fracture of Gear Teeth," *Fatigue Fract. Engng Mater. Struct.*, 23, pp. 283–292, 2000.
4. MackAldener M. and M. Olsson, "Interior Fatigue in Gear Teeth," *Proc. of Fatigue 2000*, Eds. M.R. Bache et al., Cambridge, EMAS, 2000.
5. Shulz, M., and J. Sauter, Schadenuntersuchungen an Zahnräder, Konferenz. Einzelbericht: Randschichtermüdung im Wälzkontakt, AWT-Tagung, Arbeitsgemeinschaft Wärmebehandlung und Werkstofftechnik, Suhl, D, 06.-07, 1992.
6. Alban, L., E., *Systematic Analysis of Gear Failures*, American Society for Metals, 1993.
7. ANSYS 5.5 Users manual (1998) ANSYS Inc.
8. LDP, Load Distribution Program v10.01 (1997) Ohio-State University.
9. Findley W. N., "A Theory for the Effect of Mean Stress on Fatigue of Metals Under Combined Torsion and Axial Load or Bending," *J. Engng for Industry*, November, 1959, pp. 301-306.
10. E. P. Box, W. G. Hunter and J. S. Hunter (1978), *Statistics for Experimenters*, John Wiley and Sons.
11. D. C. Montgomery (1997), *Design and Analysis of Experiments*, Fourth Edition, John Wiley and Sons.
12. K. L. Johnson (1993). *Contact Mechanics*, Cambridge University Press.